Computed Cleansing for Virtual Colonoscopy Using a Three-Material Transition Model

Iwo Serlie[1], Roel Truyen[2], Jasper Florie[3], Frits Post[4], Lucas van Vliet[1], Frans Vos[1,3]

[1] Pattern Recognition Group, Delft University of Technology, Lorenzweg 1, 2628 CJ Delft, The Netherlands 1, 2628 CJ Delft, The Netherlands, {iwo, frans}@ph.tn.tudelft.nl
[2] Medical IT - Advanced Development, Philips Medical Systems Nederland B.V., P.O. Box 10000, 5680 DA Best, The Netherlands, roel.truyen@philips.com
[3] Department of Radiology, Academic Medical Center Amsterdam, P.O. Box 22700, 1100 DE Amsterdam, The Netherlands, frans@ph.tn.tudelft.nl
[4] Computer Graphics and CAD/CAM Group, Delft University of Technology, Zuidplantsoen 4, 2628 BJ, Delft, The Netherlands, frits@ph.tn.tudelft.nl

Abstract. Virtual colonoscopy is a non-invasive technique for the detection of polyps. Currently, a clean colon is required; as without cleansing the colonic wall cannot be segmented. Enhanced bowel preparation schemes opacify intraluminal remains to enable colon segmentation. Computed cleansing (as opposed to physical cleansing of the bowels) allows removal of tagged intraluminal remains. This paper describes a model that allows proper classification of transitions between three materials: gas, tissue and tagged intraluminal remains. The computed cleansing effectively detects and removes the remains from the data. Inspection of the 'clean' wall is possible using common surface visualization techniques.

Keywords: volume segmentation, cleansing, virtual endoscopy, colonoscopy, colonography

1 Introduction

Virtual colonoscopy (also referred to as Colonography) is a non-invasive technique for the detection of polyps [4]. Polyps with a diameter larger than five mm are potentially cancerous growths and have to be removed. The early removal of these polyps reduces colorectal cancer mortality [1,5]. Virtual colonoscopy (VC) offers several advantages compared to colonoscopy: a larger range of exploration, less patient discomfort, no sedation, no risk of perforation and lower costs.

The virtual-colonoscopic procedure consists of several steps. First, a volume of the gas-distended colon is acquired using CT imaging. Second, the colon surface is segmented. Finally, a medical specialist examines the result. VC currently requires a clean colon, as without cleansing the colonic wall cannot be segmented properly. Even remains of stool and fluid could be falsely interpreted as polyps or vice versa (Fig. 1). For VC to become a clinically viable diagnosis method, accurate segmentation is essential. Cleansing includes large amounts of a laxative to empty the colon and is considered burdensome by patients.

Bowel preparation schemes have been introduced that include contrast media to opacify the intraluminal remains [6,7] (Fig. 1). Contrast enhancement assists the segmentation of intraluminal materials from soft tissues (computed cleansing) [7,2]. It potentially allows a less strict colon preparation as well [9].

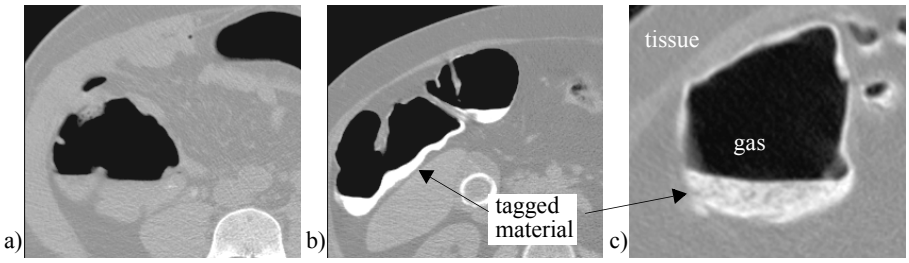

Fig. 1. CT data without opacifying contrast (a), with tagged material (b, c)

First, this paper gives a detailed analysis of the problem (section 2). In section 3, a model is described which segments partial-volume values at two- and three-material transitions into material mixtures. Results will be given in section 4 and conclusions in section 5.

2 Problem analysis and previous work

A method for computed cleansing must accurately segment the shape of the colon surface. Therefore, it must deal with the following problems:

- *partial-volume effect*. Mainly due to finite sizes of X-ray source and detectors and the point spread function (PSF) a measurement value is a weighted average of the attenuation distribution in a certain neighbourhood. In other words, the measurement process mixes materials as a consequence of which boundaries become blurred.
- *non-uniform distribution of materials*. Average CT values of contrast enhanced fluid and stool and body materials may vary (Fig. 1c).
- *noise*. The measurement process contaminates the data with noise. Specifically, low radiation dose increases noise.
- *anisotropic image data.*
- *patient-friendly bowel preparation schemes.* In new schemes extensive liquefaction of fecal materials is left out. We cannot assume that due to gravity, the fluid inside the colon gathers into concave parts creating horizontal fluid surfaces (Fig. 1b).

Thresholding is adequate to segment a properly cleansed colon [8]. However, it cannot be used to segment in the presence of contrast enhanced fluid. A thin soft-tissue-like layer would remain at the gas/fluid transition due to the partial-volume effect. Furthermore, applying a threshold assumes a uniform distribution of the opacifying contrast medium.

Many publications report on segmentation methods for virtual colonoscopy. Most of these assume that a standard cleansing procedure is followed. Wyatt et al. describe a method that uses curvature analysis to detect the gas/fluid transition [9]. Sato et al. describe a vertical filter to remove all partial-volume voxels at the gas/fluid transition [3]. The latter method is limited to binary-voxel accuracy. Both methods assume a horizontal gas/fluid boundary.

Some publications report on segmentation methods that have partial-volume accuracy. Chen et al. employ a principal component analysis on a 23-D local intensity vector [2]. However, artifacts are present at locations where gas, colon wall, and contrast

enhanced fluid are connected. Polyps of 5 mm in diameter, if located at these junctions could potentially be missed. Additionally, the method requires a homogeneous distribution of contrast material. Lakare et al. describe a cleansing method using segmentation rays [10]. Their method requires the user to carefully study and select intersection characteristics and assign classification and reconstruction tasks to the rays. Moreover, junctions of three materials are not modelled. In other words, most current segmentation methods cannot handle a less strict colon preparation scheme (Fig. 1 b, c).

Our objective is to solve the computed cleansing problem at two- and three-material transitions. A three-material transition model recovers material mixtures with subvoxel accuracy. Computed colon cleansing amounts to removing the estimated contrast enhanced stool and fluid fraction from all voxels.

3 Method

For the partial-volume effect, a model is constructed which best corresponds to the behaviour of CT values at material transitions. Subsequently, this model is fitted to the CT data, and the parameters are estimated. Finally, the model is used to calculate the material mixture in every voxel.

3.1 Partial volume effect

Let us assume three material types in a region around the colon surface: gas, tissue and contrast-enhanced (tagged) material. A CT value z is modelled as a linear combination of material contributions $\phi = a \cdot \mu_g + b \cdot \mu_t + c \cdot \mu_c$ The fraction a corresponds to gas, b to tissue and c to tagged material. These mixture fractions can be represented as barycentric positions in a triangle (Fig. 2). During acquisition these material fractions are measured as single CT values.

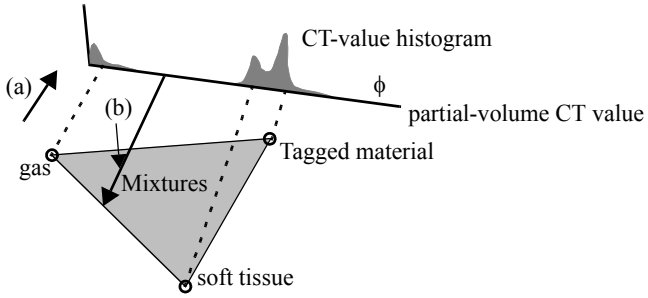

Fig. 2. Projection of material mixtures on CT values (a) and back-projection of CT values (b).

The following sections explain how to perform the inverse operation: determine material mixtures starting from the acquired CT values (Fig. 2b).

3.2 Two-material transition model

Model building. A transition between two materials is modelled as a Gaussian smoothed step edge with variance σ^2 (the cumulative-Gaussian distribution). Let ϕ represent a CT value and $|\nabla\phi|$ the gradient-magnitude. Plotting $|\nabla\phi|$ as a function of ϕ yields an arch-shaped curve. Henceforth, it is referred to as the A-curve (Fig. 3b). Note that ϕ is linearly dependent on material fractions (Section 3.1).

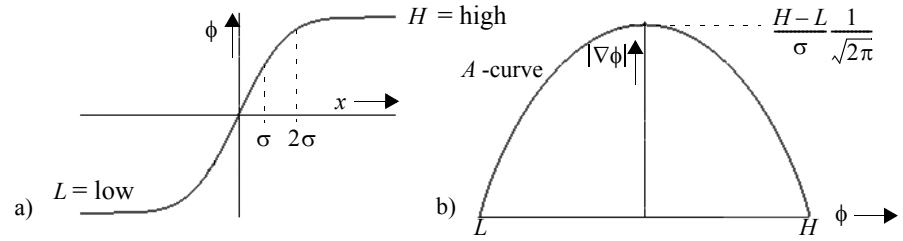

Fig. 3. CT value (a) CT value and Gradient magnitude model of a two-material transition (b).

Consider the general definition of the Gaussian and the error function (Eq. 1). A closed formula of the A-curve (Eq. 2) is defined with a limited number of parameters: two-constant CT values at the step-edge L, H (Fig. 3a) and the σ of the Gaussian.

$$g(x) = \frac{1}{\sqrt{2\pi}} e^{\frac{-x^2}{2}}, \quad erf(z) = \frac{1}{\sqrt{\pi}} \int_0^z e^{-t^2} dt, \tag{EQ 1}$$

$$A(\phi;(L, H, \sigma)) = \frac{H-L}{\sigma} g\left\{ \sqrt{2} erf^{-1}\left(2\frac{\phi - L}{H-L} - 1\right)\right\} \tag{EQ 2}$$

The A-curve models the behaviour of CT derivatives near material transitions as function of ϕ.

Determination of model parameters. Let us focus on the example profile crossing three two-tissue transitions (Fig. 4). Walking along the line from top to bottom, the position on the A-curves are traced. Observe the three A-curves that occur at the three types of transitions: tissue/gas, gas/tagged material and tagged material/ tissue.

Three models are defined by choosing the parameters (L, H, σ) that best fit the three types of transitions. The parameters are determined by the following procedure:

1. For every voxel CT values (ϕ, $|\nabla\phi|$) are sampled in the direction of the gradient at the voxel. Note that we only need to sample in the immediate neighbourhood of the current voxel.
2. Determine the A-curve parameters that best fit to these CT measurements and collect the L and H parameters in a 2-D histogram (Fig. 5). The L-parameter is plotted on the horizontal axis and the H-parameter on the vertical axis.
3. The average values of gas, tissue and contrast enhanced fluid are determined from the 2-D histogram (Fig. 5b). In the L-direction the first top corresponds to air. Restricting the range of values in the H-direction to this value, the first top corresponds to tissue and the second top to tagged material. The σ is estimated by averaging all A-curve σ estimates (it is assumed that the point spread function is isotropic).

Now we have models for the CT value characteristics for each of the three transitions. It enables us to determine the material contributions per voxel as follows.

Determining the material mixtures. First, CT measurements (ϕ, $|\nabla\phi|$) are sampled in the direction of the gradient in the immediate neighbourhood of the voxel.

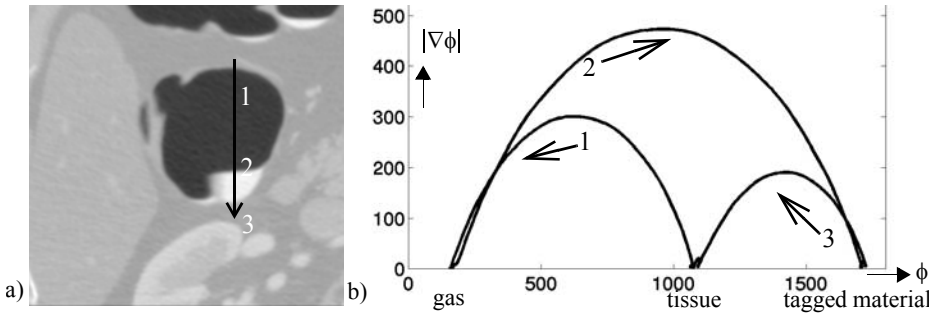

Fig. 4. Profiles (a) with corresponding curves in (CT value, CT gradient magnitude) space (b).

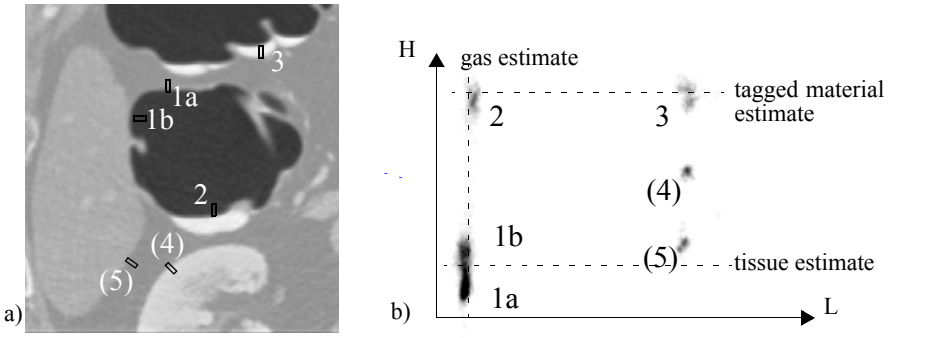

Fig. 5. Typical CT slice (left) with corresponding L, H histogram of CT values (right). Partial-volume values are not plotted because they do not occur near the A-curve ϕ -axis (Fig. 3c).

Subsequently, the A-curve and position that best fits these local measurements is selected (Fig. 6). Finally, the material fractions are determined as shown.

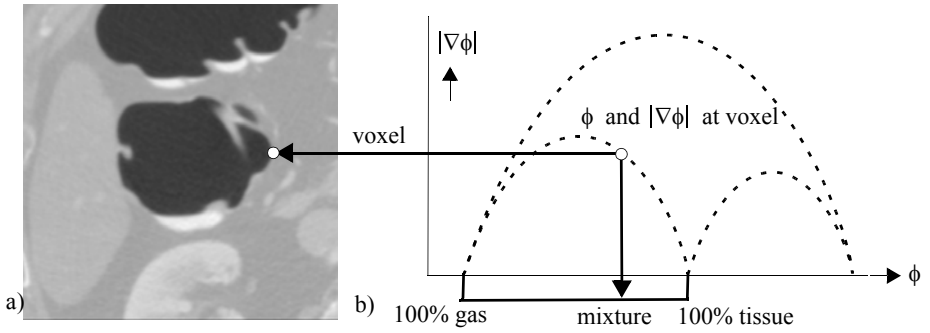

Fig. 6. Calculating the tissue mixture using the two-material transition model at a voxel.

Thus far we have focused on determining partial-volume contributions at two-material transitions. Such a description is not sufficient to solve the classification problem at locations where gas, tissue, and tagged material meet. The description of the three-material transition model is analogous to the description of the two-material transition model.

3.3 Three-material transition model

Model building. The A-curve model is extended to a three-material transition model between air, tissue and tagged material. The gas/tagged material transition is modelled to intersect the tissue transition at an angle α. (Fig. 7).

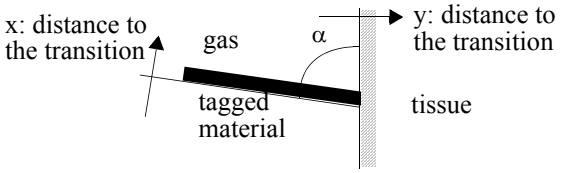

Fig. 7. Configuration of two-material transitions at a junction.

The extended model describes the behaviour of $\phi' = |\nabla\phi|$, $\phi'' = |\nabla\phi'|$ and $\phi''' = |\nabla\phi''|$ as function of the distances x, y, angle α and the σ (modelling the PSF) (Fig. 7). First, the step-edges at the junction above (Fig. 8a) are convolved with a Gaussian (σ). Each position around the junction (Fig. 7) corresponds to a material fraction captured by barycentric positions (Fig. 2). Convolving the step-edges at a junction with a Gaussian derivative filter gives the gradient-magnitude (Fig. 8b). Plotting the CT gradient-magnitude $|\nabla\phi|$ against barycentric coordinates yields a parachute-shaped surface. Henceforth it is referred to as the P-surface (Fig. 8c). Much in the same way ϕ'' and ϕ''' are determined per barycentric position.

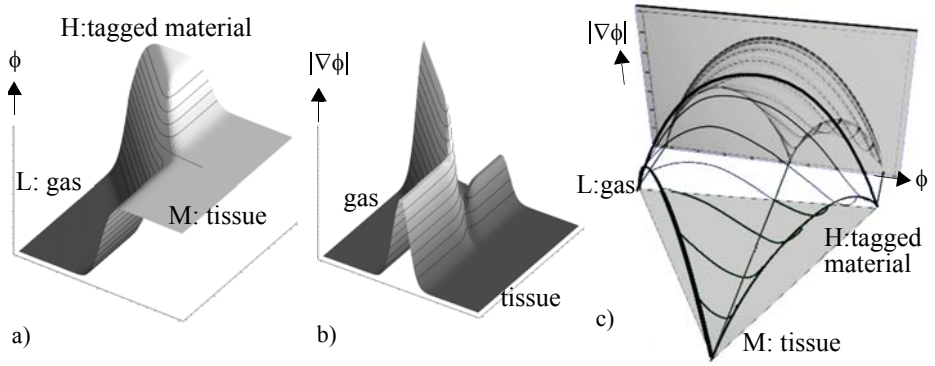

Fig. 8. CT value (a) and gradient-magnitude (b) at smoothed junction (a). Gradient magnitude model for barycentric coordinates: parachute shaped surface (P-surface) (c).

Model fitting. The CT values L, M and H that correspond to air, tissue and tagged material as well as the σ are determined using the A-curves as described above (notice that there are less junctions than edges in the data). The angle φ is set to 135 degrees roughly matching the adhesive forces at junctions (Fig. 2a).

Determining the tissue mixtures. First, CT measurements (ϕ, ϕ', ϕ'' and ϕ''') are sampled in the direction of the gradient in the immediate neighbourhood of the voxel.

Then, the position at the P-surface that best fits to these local measurements (in a least squares manner) determines the barycentric position (Section 3.1).

3.4 Robustness to noise

CT measurements at voxel positions are acquired by convolving with Gaussian kernels and interpolated using cubic spline interpolation. A sufficiently sized σ and sample trajectory in the gradient direction makes the method robust to noise. The resolution of significant colon surface details (set to a diameter ≥ 5 mm) determines the maximum size of the kernels. Typical values are $\sigma = 1 \ldots 2$ mm and a distance of 0.3 mm in the direction of the gradient.

4 Evaluation and results

4.1 Patient inclusion

The performance of computed cleansing was measured by a retrospective study. Five consecutive patients with nine polyps larger than five mm in diameter were selected from an ongoing study. The main patient inclusion criterion was the referral for optical colonoscopy.

A less strict bowel preparation scheme was used that included oral contrast agents. Two days before image acquisition, the patient was asked to take a contrast medium with each meal (low-fibre). Oral lactulose was included for stool softening. Prior to the scan the colon was distended with CO_2 enriched room air. The multi-slice CT scan (using the Philips-Mx8000, Best, The Netherlands) was acquired two to four weeks before the colonoscopy. The protocol included 50 to 70 mAs and a scan time of 20 to 25 seconds. The reconstructed data were 250 to 300 3.2 mm thick 512x512 images.

Identified polyps were resected and their size, location and morphology were annotated to define the ground truth.

The computed cleansing method was implemented on an experimentally enhanced version of the EasyVision software (Philips Medical Systems).

4.2 Polyp observation

Nine polyps were retrospectively examined by one medical specialist. First, the polyps were observed using 2-D uncleansed data and second, using 2-D computed cleansed data. Each polyp was classified into four classes: (1) Clearly visible, (2) visible, but can be missed, (3) retrospectively clearly visible, but can be missed prospectively and (4) not retrospectively visible.

Using both uncleansed data and cleansed data, seven out of nine polyps were annotated as clearly visible in the supine position and five out of nine polyps as ‘clearly visible’ in the prone position. Three polyps were annotated as ‘retrospectively clearly visible, but can be missed prospectively’ using the 2-D uncleansed data. They were annotated as ‘clearly visible’ using the computed cleansing procedure.

From the included polyps three are selected to illustrate typical problems. The first image shows a non-horizontal gas/tagged material surface that covers a polyp (Fig. 9). The next figure illustrates the segmentation of high intensity stool in the rectum (Fig. 10). Finally, the third figure demonstrates a small fraction that is deposited in a haustra (Fig. 11).

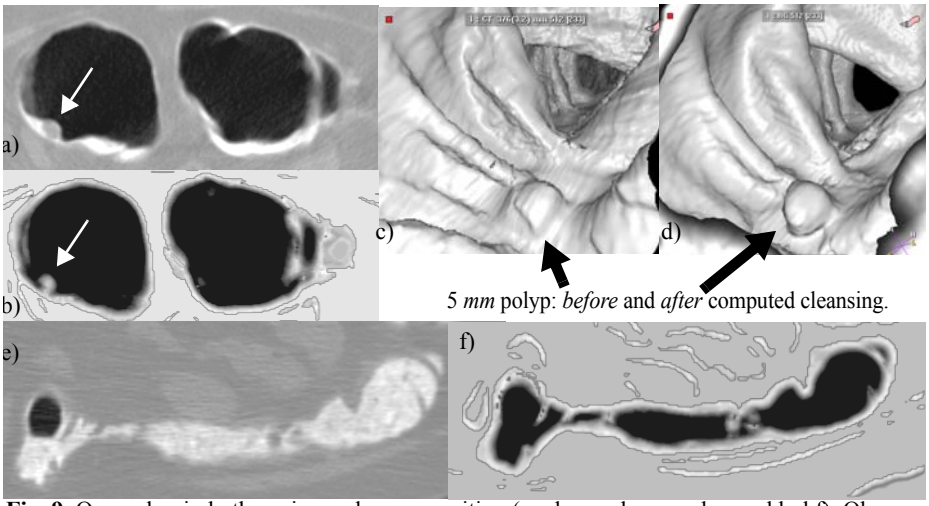

Fig. 9. One polyp in both supine and prone position (uncleansed a,c,e; cleansed b,d,f). Observe that computed cleansing improves the overall surface quality because the method compensates for tissue inhomogeneities and noise as well.

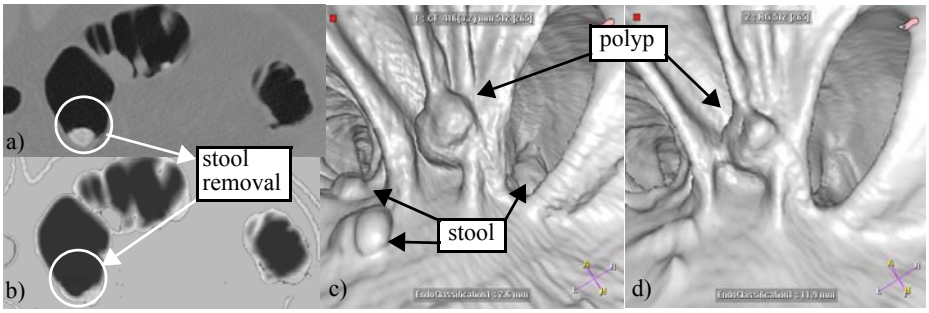

Fig. 10. One polyp in the sigmiod of 1 cm. It can be observed that three stool sections are removed from the data.

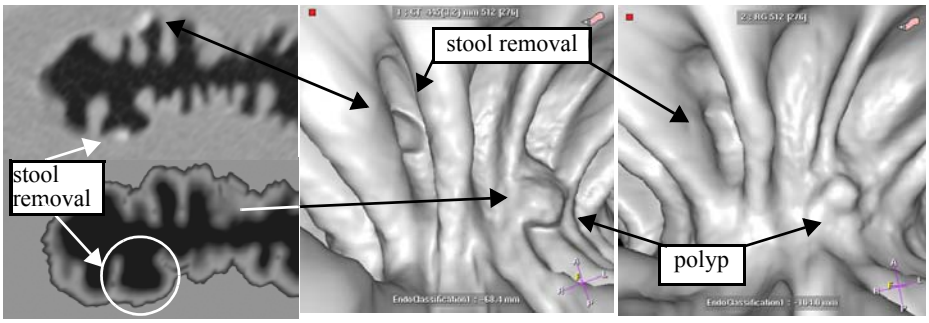

Fig. 11. One polyp in the transversum of approximately 5 mm. Observe the polyp-like shape in the haustra that is removed by computed cleansing.

Additionally, the following example shows a manual segmentation within uncleansed data that also is depicted in cleansed data.

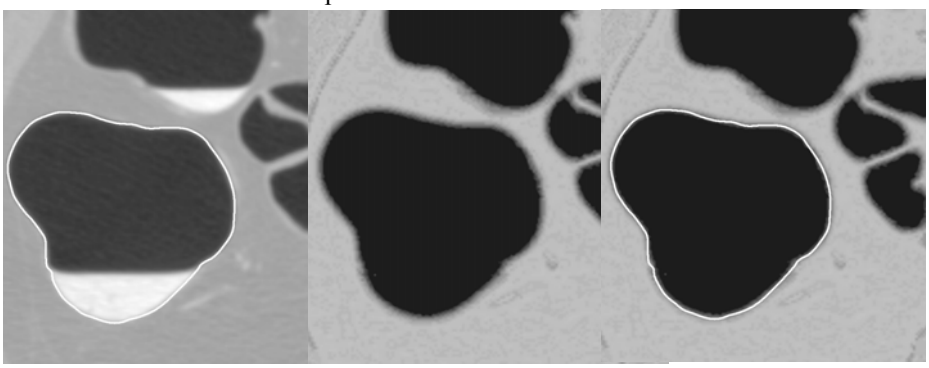

Fig. 12. Manual segmentation compared to computed cleansing.

5 Conclusion

This paper reports on progress in computed colon cleansing. It enables a scheme with a less strict bowel preparation.

The method successfully handles three-material transitions. It uses the partial-volume effect to classify materials. Material inhomogeneities are handled properly by incorporating higher order derivatives into the model. The method is robust to noise due to the filtering in the Gradient-direction. Thus, using existing surface visualization techniques the localization of the iso-surface is improved.

The evaluation shows promising results on polyp observation. The evaluation time is not recorded. We expect much shorter evaluation times using the computed cleansing method, because the medical skilled person is only involved in inspecting tissue without having to segment the data mentally.

Omitting the laxatives, the proposed method enables virtual colonoscopy to become the method of choice for large-scale diagnosis and screening.

6 References

[1] Parker, T.Tong, S. Bolden, P.Wingo, “Cancer statistics 1997”, CA Cancer Journal for Clinicians 47, pp. 5-27, 1997.

[2] Chen, D., Liang, Z., Wax, M., Li. L., Li, B., Kaufman, A., “A Novel Approach to Extract Colon Lumen from CT images for Virtual Colonoscopy”, IEEE transitions on medial imaging, Vol. 19, No. 12, pp. 1220-1226, December 2000.

[3] Sato, M., Lakare, S., Wan. M., Kaufman, A., Liang, Z., Wax.M., “An automatic colon segmentation for 3D virtual colonoscopy, “IEICE Trans, Information and Systems, Vol. E84-D, No. 1, January 2001, pp. 201-208.

[4] Vining, D., Gelfand, D., Bechtold, R., Scharling, E., Grishaw, E., Shifrin, R., "Technical feasibility of colon imaging with helical CT and virtual reality", Proc. Ann. Meeting of Amer. Roentgen Ray Soc., p. 104, 1994.

[5] Mandel, J., Bond, J., Church, J., Snover, D., “Reducing Mortality from Colon Cancer Control Study”, New England J Med 328, pp. 1365-1371, 1993.

[6] Liang, Z., Yang, F., Wax, M., Li, J., Kaufman, A., Hong, L., Li, H., Viswambharan, A., “Inclusion of A priory Information in Segmentation of Colon

Lumen for Virtual Colonoscopy, Conf Record IEEE NSSS-MIC, CD-ROM, 1997.
[7] Wax, M., Liang, Z., Chen, D., Li, B., Chiou, R., Kaufman, A., Viswambharan, A., “Electronic Colon Cleansing for Virtual Colonscopy”, 1st Intl Conference on Virtual Colonoscopy, Boston, MA, October 1998.
[8] Hong, L., Kaufman, A., Wei, Y., Viswambharan, A., Wax, A., Liang, Z., “3D Virtual Colonoscopy”, Proc. Symposium on Biomedical Visualization”, pp. 26-32, 1995.
[9] Wyatt, C.L., Ge, Y., Vining, D.J., "Automatic Segmentation of the Colon for Virtual Colonoscopy", Comp Med Im Graph, 2000; 24: 1-9.
[10] Lakare, S., Wan, M., Sato, M., Kaufman, A., "3D Digital Cleansing Using Segmentation Rays”, IEEE Visualization 2000 Conference Proceedings, ACM/ SIGGRAPH, Press, pp. 37-44, October 2000.

7 Acknowledgements

We would like to thank Dr. P. Rogalla, Charité Berlin, for providing us with tagged patient data. Additionally, we would like to thank Dr. J. Stoker, Academic Medical Center Amsterdam, for sharing with us tagged patient data from an ongoing study.